Chemical Geology 662 (2024) 122234

Contents lists available at ScienceDirect

Chemical Geology

journal homepage: www.elsevier.com/locate/chemgeo

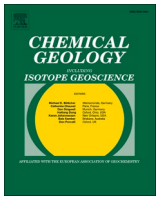

Nickel's behaviour in marine sediments under aerobic to anaerobic diagenetic conditions

Sylvie Bruggmann [a,b,*], James McManus [c], Corey Archer [d], Derek Vance [d], Silke Severmann [a]

[a] Rutgers University, Department of Marine and Coastal Sciences, 71 Dudley Road, New Brunswick, NJ 08901, USA
[b] University of Lausanne, Institute of Earth Sciences, Quartier UNIL – Mouline, Géopolis, 1015 Lausanne, Switzerland
[c] Bigelow Laboratory for Ocean Sciences, 60 Bigelow Drive, East Boothbay, ME 04544, USA
[d] ETH Zurich, Department of Earth Sciences, Clausiusstrasse 25, 8092 Zürich, Switzerland

ARTICLE INFO

Editor: Vasileios Mavromatis

Keywords:
Ni isotopes
Pore water
Early diagenesis
Marine Ni cycle

ABSTRACT

In the marine environment, nickel distributions are linked to the biogeochemical cycling of both organic matter and manganese. Thus, Ni and its isotopes have the potential to be used to reconstruct changes of bioproductivity and oxygenation in paleoenvironments. However, their utility relies on an understanding of the behaviour of Ni in modern marine environments. Here we investigate the distribution of Ni under a range of oxidation-reduction conditions, with organic carbon (C_{org}) burial rates that range from approximately 0.08 to 8.4 mmol m^{-2} d^{-1}, none of the sites show deep (> 5 cm) penetration of dissolved oxygen into the sediment. We present Ni concentrations for sediments and pore fluids, as well as Ni isotope compositions from pore fluids, from the California and Mexico continental margins. The sites are sufficiently reducing that solid-phase Mn concentrations are typically <1000 ppm, but two of the stations, where oxygenated bottom water bathes the underlying sediment, have near-surface sediment Mn concentrations that reach up to 2.3%.

Dissolved Ni is lower in pore fluids for stations with high solid phase C_{org} compared to those stations with oxygenated bottom water and high solid phase Mn concentrations. The calculated benthic fluxes of Ni at all stations are small relative to their burial rates, which implies a high Ni burial efficiency (> 85%). Pore fluid δ^{60}Ni values range from approximately −0.39 to +2.36 ‰, with the higher δ^{60}Ni values occurring at the C_{org}-rich station, and the lower values at the Mn-rich stations. At the station with the highest C_{org} content, the distribution of solid-phase Ni as a function of C_{org} content is consistent with the strong association of Ni with C_{org} seen at open-ocean upwelling margins globally. In contrast, the other stations investigated here clearly do not show such an association. Our data offer support for the notion that Ni accumulation within sediments is linked to organic matter accumulation in regions of high photic zone productivity and where the sediments are reducing. However, at the sites in our study where Mn oxidation-reduction reactions occur near the sediment-water boundary, any simple relationship between Ni and C_{org} burial is obfuscated. With a sufficiently deep oxygen penetration depth and the formation of a solid-phase Mn oxide layer, Ni burial within the sediment can be highly efficient. Importantly, Ni is well preserved in sediments deposited under the full range of conditions studied here. This observation of high Ni preservation is an important constraint if Ni is to be used as a proxy to reconstruct paleoenvironmental conditions.

1. Introduction

Nickel is a bioactive metal that is essential for the metabolism of organisms, particularly for enzymes involved in nitrogen metabolism (e.g., Bruland, 1980; Ragsdale, 2009; John et al., 2022; Lemaitre et al., 2022). Within the oceanic water column, Ni shows a distribution analogous to a number of macronutrients, with low (as low as about 2 nM) concentrations at the surface and higher concentrations (up to 10 nM) in deep water (e.g., Bruland, 1980; Mackey et al., 2002; Archer et al., 2020). Although not depleted to near-zero concentrations like many other bioactive metals, (e.g., Cd, Fe, Zn), low concentrations of Ni in the surface ocean have been suggested to limit phytoplankton growth (e.g., Sclater et al., 1976; Bruland, 1980; Boyle et al., 1981; Mackey et al., 2002; Archer et al., 2020; Yang et al., 2021; John et al., 2022), possibly

* Corresponding author.
E-mail address: sylvie.bruggmann@unil.ch (S. Bruggmann).

https://doi.org/10.1016/j.chemgeo.2024.122234
Received 26 February 2024; Received in revised form 8 June 2024; Accepted 13 June 2024
Available online 14 June 2024

due to strong complexation of a portion of the photic zone pool, rendering it non-bioavailable (Mackey et al., 2002; Archer et al., 2020). However, significant uncertainties persist concerning Ni cycling in modern marine environments, particularly regarding its behaviour during the earliest phases of diagenesis.

In addition to its association with organic carbon (C_{org}), Ni is coupled to the behaviour of Mn, which itself is related to C_{org} cycling via electron donor and acceptor interactions (e.g., Shaw et al., 1990; Atkins et al., 2016). Positively charged Ni ions readily adsorb onto negatively charged surfaces of Fe and Mn oxides (Koschinsky and Hein, 2003). Laboratory experiments have demonstrated that surface-bound Ni can migrate via diffusion until it is structurally incorporated into Mn oxides, such as birnessite (Peacock, 2009). In natural Mn oxides, Ni can also be structurally incorporated rather than being surface-bound (Peacock and Sherman, 2007). Regardless of its mechanistic association with Mn, the oxidation and reduction processes that occur in near-surface marine sediments have the potential to concentrate Ni, either in the dissolved phase, through Mn dissolution, or the solid phase, through Mn precipitation (e.g., Shaw et al., 1990). Nickel can also be associated with Fe-rich sediment phases, including Fe sulfides (FeS), Fe(oxyhydr)oxides or Fe-rich clays (e.g., Hein et al., 1979; Landing and Lewis, 1991; Stumm and Morgan, 1996).

The strong associations between Ni and C_{org} and Mn oxides result in sediments that are rich in these phases being the dominant sinks for Ni in the modern ocean (e.g., Tribovillard et al., 2006; Cameron and Vance, 2014; Böning et al., 2015; Gueguen et al., 2016, 2018; Ciscato et al., 2018; Little et al., 2020; Gueguen and Rouxel, 2021; Fleischmann et al., 2023). In the case of C_{org}-rich sediments, which typically lie below regions of high biological production, Ni accumulation is attributed to delivery in association with settling organic matter (Böning et al., 2015; Ciscato et al., 2018). Likewise, because Mn is delivered to the sea floor with settling particulate material (e.g., Johnson et al., 1996), Ni will also be delivered via its association with Mn. Once at the seafloor, particularly where C_{org} rain rates are high, the lack of dissolved oxygen and low nitrate concentrations within the sediment package facilitate the release of Ni from the initial solid phases.

The Ni isotope system has received increasing attention recently, including in the marine realm (e.g., Cameron and Vance, 2014; Vance et al., 2016; Gueguen et al., 2016, 2018; Takano et al., 2017; Wang et al., 2019; Ciscato et al., 2018; Archer et al., 2020; Little et al., 2020; Yang et al., 2020, 2021; Gueguen and Rouxel, 2021; Lemaitre et al., 2022; He et al., 2023; Fleischmann et al., 2023). The distribution of Ni isotopes in the modern ocean appears to be characterised by a biogeochemical divide. While the deep ocean and surface waters north of the Subarctic Front show rather homogeneous Ni concentrations and δ^{60}Ni values, surface waters of low-latitude regions show increased δ^{60}Ni values associated with the lowest Ni concentrations, a feature that has been linked to isotope fractionation associated with N_2 fixation (Lemaitre et al., 2022).

Despite recent advances in the understanding of Ni isotope behaviour in the modern water column (e.g., Archer et al., 2020; Yang et al., 2021; Lemaitre et al., 2022) and at the sediment-water interface (e.g., He et al., 2023; Fleischmann et al., 2023), the database for Ni concentrations and isotope compositions in sediments, pore fluids and the water column remains limited. This study contributes to the understanding of Ni in marine environments by investigating sites with differing dominant modes of electron transport. Under these environmental conditions, we examine the processes affecting Ni and its isotope values during early diagenesis. While the distribution of a range of trace metals, including Ni, has been described by Shaw et al. (1990) for three of the stations investigated here, we add new pore fluid Ni isotope data, and re-examine the extended data set of sediments and pore fluids.

2. Material and methods

2.1. Sampling sites

Our sampling sites are located within an upwelling zone along the California and Mexico continental margins (Fig. 1). These stations have a range of bottom water oxygen concentrations, C_{org} burial and mass accumulation rates (MAR; Table 1). The geology and geochemistry of these sites have been characterised extensively elsewhere (e.g., Berelson et al., 1987; Shaw et al., 1990; McManus et al., 2006; Chong et al., 2012; McManus et al., 2012).

The Mexico site (Soledad) is within the Eastern Tropical North Pacific OMZ (see McManus et al., 2006). At this site, bottom water oxygen concentrations are <0.1 μM and the C_{org} burial rate is high (8.4 mmol m^{-2} day^{-1}; McManus et al., 2006). Previous work at Soledad has shown that pore fluid dissolved H_2S concentrations increase with depth, from approximately 7 μM close to the sediment-water interface up to 42 μM at 9.5 cm sediment depth (Supplementary Material Table S1; Chong et al., 2012). Furthermore, Soledad has high dissolved Fe concentrations near the sediment surface that decrease with depth, reaching values that are below the detection limit by 9.6–10.8 cm sediment depth, which coincides with an increase in dissolved sulfide concentrations (Chong et al., 2012).

The California sites, which include the Catalina Basin and San Clemente, and the off-shore Patton Escarpment, underlie the California current system (McManus et al., 1997). At water depths between 500 and 1000 m, the oxygen minimum zone bathes the sediment along this continental margin (McManus et al., 1997). The submarine basins of the inner continental margin have restricted water and chemical exchange that influences the chemical character of each basin (e.g., Sholkovitz, 1972; Berelson et al., 1987; Shaw et al., 1990). Bottom water oxygen concentrations vary depending on the depth of the sill relative to the oxygen minimum zone and the C_{org} rain rate, as does oxygen consumption in deep water or within the sediment package (Berelson et al., 1987; McManus et al., 1997; Shaw et al., 1990). These sites span a range of bottom water oxygen concentrations between 19 and 132 μM and have C_{org} burial rates that range from 0.08 to 1.2 mmol m^{-2} day^{-1} (Berelson et al., 1996; McManus et al., 2006). In Catalina Basin, San Clemente, and at the Patton Escarpment, oxygen penetrates the sediment to ~0.3 cm, ~1.3 cm and ~2.9 cm, respectively (Berelson et al., 1996 and references therein). Because oxygen is present in bottom water and penetrates the upper surface sediment, the California sites are hereafter referred to as the "oxic" sites. The sediments of the San Clemente Basin and those along the Patton Escarpment are also enriched in solid-phase Mn (McManus et al., 2006). This enrichment is likely driven by the deeper penetration of dissolved oxygen compared to the more reducing sites. In short, the penetration of oxygen into the upper

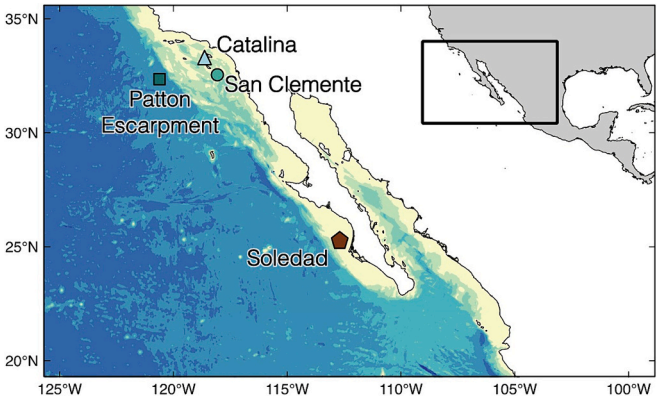

Fig. 1. Map showing the sampling sites for this study (GEBCO Compilation Group (2020) GEBCO 2020 Grid).

Table 1
Geographic locations and information on oxygen content, organic matter burial and mass accumulation rates.

Location		Depth	°N	°W	BW O_2	O_2 penetration[a]	C_{org} burial[b]	MAR[c]
		m			μM	cm	mmol m^{-2} d^{-1}	mg cm^{-2} y^{-1}
Soledad	Mexico	430	25.2	112.7	<0.1		8.4	50
Catalina Basin	CA, USA	1300	33.3	118.6	19	0.33	1.2	14
San Clemente	CA, USA	2053	32.6	118.1	52	1.28	0.9	15
Patton Escarpment	CA, USA	3707	32.4	120.6	132	2.87	0.08	3

[a] Berelson et al., 1996
[b] McManus et al., 2006
[c] MAR = sediment mass accumulation rate; McManus et al., 2006; Poulson et al., 2006

few mm to cm of sediment fosters precipitation of reduced Mn that diffuses upward into the oxidised layer from below, where Mn is undergoing reductive dissolution (McManus et al., 2006).

2.2. Sample collection and preparation and TOC analysis

Sediment and pore fluid samples at these stations were collected with a multi-corer during a research expedition in May/June of 2018 (Barnett et al., 1984). The samples were processed *on board* under anoxic conditions and in a temperature-controlled cold room.

Pore fluid samples were collected from sediment cores by sequentially loading sediment into 85 cm^3 polycarbonate centrifuge tubes down to a depth of ~10 cm, and pore fluids were extracted using traditional centrifugation techniques under anaerobic conditions. Each centrifuge tube nominally represents an interval of approximately 1.2 cm and data are presented as the mid-point of each interval. Centrifuge sample supernatants were filtered with 0.45 μm filters and acidified to a pH of ≈ 1.8 with HCl for storage.

Solid phase sediment was collected separately by slicing a core in 1 to 2 cm increments and the data are presented as the mid-point of a sediment interval. Directly after slicing, sediment samples were placed in plastic freezer bags and the samples were then frozen. The sediment samples were freeze-dried and powdered before further processing.

Sediment samples were digested following a standard procedure for marine sediment digestion, including incineration and dissolution with a mixture of HF and HNO_3. Samples that contained solids (Al fluorides) after treatment with HF and HNO_3 were heated in 12% HNO_3 at 60 °C for 36 h (Muratli et al., 2012). Total organic carbon (TOC) contents were analysed on a GVI (now Elementar) Isoprime 1000 with Eurovector EA at Bigelow Laboratory for Ocean Sciences. The uncertainties of TOC analyses are between 0.1 and 0.4% C (see also Bruggmann et al., 2023).

2.3. Concentration analyses

Aliquots of pore fluids were diluted to determine concentrations on a Thermo Scientific Element XR at ETH Zurich. These concentrations were used to estimate the appropriate volume of Ni double spike. Final Ni concentrations of pore fluids were calculated using isotope dilution as part of the double spike isotope analysis (Thermo Scientific Neptune Plus, ETH Zurich; see Section 2.4).

Solid-phase Ni concentrations were analysed using an iCap collision cell ICP-MS Thermo Fisher (Rutgers University). A shale standard reference material (SDo-1, Devonian shale) gave an average Ni concentration of 98.1 ± 11 ppm (SD, $n = 4$), compared with the certified concentration of 99.5 ± 10 ppm (SD).

2.4. Nickel isotope analysis

Nickel isotope analyses were carried out following previously published procedures at the ETH Zurich laboratories (Cameron and Vance, 2014; Little et al., 2014; Archer et al., 2020; Sun et al., 2021; Lemaitre et al., 2022), and only important modifications from the above are described in detail below. The main modification employed here was during the pre-concentration of Ni from the porewater fluids. Aliquots of between 5 and 45 ml of pore fluids were spiked with a ^{61}Ni—^{62}Ni double spike at a sample:spike ratio of approximately 1. After spike equilibration, Ni was pre-concentrated using an ethylenediaminetriacetic acid chelating resin, Nobias PA1 (Hitachi High Technologies), seated in gravity flow columns (Sun et al., 2021). Here the sample is loaded in a solution buffered to pH 5 with 0.1 M ammonium acetate onto a resin bed (9 mm long by 6 mm inner diameter). The low aspect ratio of this column was designed specifically to allow re-suspension of the Nobias resin after sample chelation, required to maintain an adequate flow-through of the sample solution. Nickel was then purified from the resultant trace metal mixture, first via an anion exchange resin (AG MP-1 M, Bio-Rad) to isolate Ni from other transition metals. The Ni fraction was then further purified using a second pass of the gravity-driven Nobias column, to remove any residual Na, Mg or Ca. Finally, the Ni fraction was then passed through a second, small, anion column to remove any residual Fe or Zn. Typical procedural Ni blanks for this multi-step protocol are <0.5 ng.

Isotope compositions were analysed using a multi-collector ICP-MS (Thermo Scientific Neptune Plus) at ETH Zurich. Prior to analysis, the purified Ni samples were refluxed in an $HNO_3 + H_2O_2$ mixture to oxidise and eliminate residual organic matter. Samples were re-dissolved in 2% HNO_3 (v/v ~ 0.3 M) and typically run at 100 ppb Ni. The samples were introduced with a Savillex C-Flow PFA nebuliser (50 μl min^{-1}) via a Teledyne-Cetac Aridus II desolvator. Analyses were performed in low-resolution mode, using N_2 gas to suppress the formation of molecular interferences. To detect potential ^{58}Fe interferences on ^{58}Ni, masses ^{56}Fe and ^{57}Fe were monitored. For a more complete discussion on the importance of robust interference monitoring for Ni isotope analysis, see Sun et al. (2021).

The Ni double spike was used to correct for instrumental mass fractionation. Isotope compositions of Ni are reported relative to the NIST SRM 986 Ni standard in the usual delta notation (Eq. 1).

$$\delta^{60}Ni = \left(\frac{\left(^{60}Ni/^{58}Ni\right)_{sample}}{\left(^{60}Ni/^{58}Ni\right)_{SRM986}} - 1 \right) * 1000 \quad (1)$$

The long-term reproducibility of Ni isotope analyses was assessed by repeat analyses of natural standards (USGS Fe—Mn nodules, Nod-A1 and Nod—P1). The natural Ni standards give $\delta^{60}Ni = 1.04 \pm 0.07$ ‰ (2SD, $n = 228$ over 2 years) and $\delta^{60}Ni = 0.34 \pm 0.07$ ‰ (2SD, $n = 168$ over 2 years) for Nod-A1 and Nod—P1, respectively. These values overlap with the reproducibility during an individual analytical session ($n = 5$ for each of the nodules), and are in agreement with published values (Gueguen et al., 2013). The internal errors generated during an individual analysis are generally low and we report long-term reproducibility as uncertainties, unless internal errors are higher.

2.5. Diffusive benthic fluxes and Ni MAR

Diffusive benthic fluxes of Ni were calculated using Fick's first law of diffusion

$$benthic\ flux = -\phi * D_{sediment} * \frac{d[C]}{dx} \quad (2)$$

using the average porosity (ϕ; McManus et al., 2005). The concentration gradient ($d[C]/dx$) is estimated as a linear gradient between the bottom water value and the value of the uppermost pore fluid sample (0 to 1.2 cm sediment depth). For dissolved Ni concentrations in bottom water, we use the value of 10 nM as an upper limit on the concentration. This value is based on oceanographic data for the Pacific (Bruland, 1980) because we do not have an independent estimate from this study. Based on the dissolved profile within the ocean, it is likely that this value is an overestimate, but is nevertheless demonstrative for our study. The diffusion coefficient in the sediment ($D_{sediment}$) was calculated as

$$D_{sediment} = \frac{D_{seawater}}{\theta^2} \quad (3)$$

The diffusion coefficient of Ni^{2+} in seawater ($D_{seawater}$) was taken from Li and Gregory (1974). The tortuosity was derived using the relationship between porosity and tortuosity (θ^2; Boudreau, 1996).

$$\theta^2 = 1 - ln(\phi^2) \quad (4)$$

Sediment mass accumulation rates of Ni (Ni MAR) were calculated using published MAR from McManus et al. (2006) and Poulson et al., 2006, Table 1). Published MAR were multiplied by Ni concentrations averaged over the upper 10 cm of the sediment. The burial efficiency of Ni was calculated after Berelson et al. (1996) as

$$burial\ efficiency = \frac{Ni\ MAR}{Ni\ MAR - benthic\ flux} \quad (5)$$

3. Results

3.1. Anoxic environment: soledad

The Soledad station on the Mexican continental margin is anoxic and C_{org}-rich, with TOC concentrations roughly between 7 and 8 wt%, and increasing pore fluid H_2S with depth (Fig. 2; Supplementary Material Tables S1 and S2; Chong et al., 2012). For this Soledad station, Ni and C_{org} concentrations fall on the tight correlation found for sediments along the Peru and Namibia upwelling margins (Fig. 3), with sediment Ni concentrations of approximately 45.5 ± 8.5 ppm (SD) or average Ni/Al * 10^{-3} of approximately 1.61 ppm/ppm (Fig. 4). These Ni/Al ratios are high compared with the highest estimate of detrital Ni/Al in Böning et al. (2012), who estimated a range between 0 and 3.3 *10^{-4} (ppm/ppm). Calculated authigenic Ni fractions ($Ni_{auth} = Ni_{total} - (Ni/Al_{detrital} * Al_{total})$, using the maximum estimate for detrital Ni contributions (Böning et al., 2012), suggests that this fraction consists of a minimum of 78% of the total Ni (Table S2).

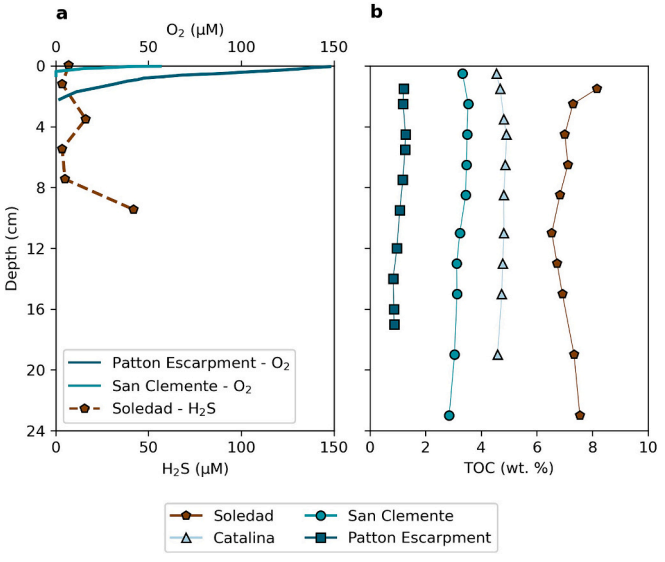

Fig. 2. a) Distributions of porewater dissolved phase O_2 and H_2S, plotted as functions of depth below the sediment-water interface. The dissolved O_2 and H_2S data are from Chong et al. (2012). b) Concentrations of total organic carbon (%) in the sediment, shown as a function of sediment depth.

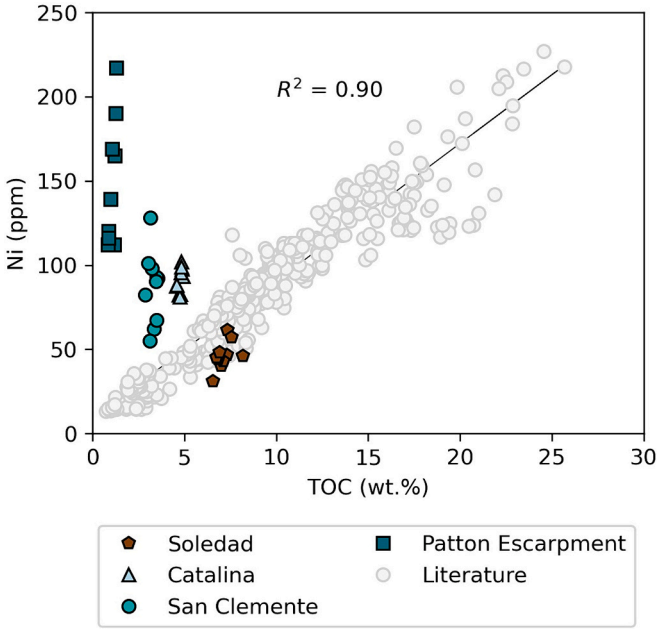

Fig. 3. Nickel concentrations in the sediments studied here, plotted as a function of TOC concentrations, and compared to literature data for the Peru and Namibia upwelling margins from Böning et al. (2015), Ciscato et al. (2018) and He et al. (2023). The data from Soledad are consistent with the data array for C_{org}-rich sediments from these other localities. The sites with lower C_{org} contents have higher Ni concentrations in the solid phase, suggesting that Ni behaviour at these sites is impacted by additional processes.

Dissolved Fe concentrations in pore fluids decrease from 57.9 μM at the surface to around 1 μM at 7.2–8.4 cm and below, while dissolved Mn is consistently below 0.2 μM (Fig. 5; Supplementary Material Table S3). Dissolved Ni concentrations are elevated over bottom water values and show only a slight increase with depth (from 39 nM to 52 nM between 0–1.2 and 10.8–12.0 cm; Fig. 6). The MAR of Ni at the Soledad station is ≈ 37 nmol cm^{-2} y^{-1} (Table 2). The net benthic Ni efflux calculated according to Eqs. 2 to 6 is −2.8 nmol cm^{-2} y^{-1} (with negative being out of the sediment), and the burial efficiency is 0.93 (Table 2). Dissolved Ni isotope compositions increase by approximately 1 ‰ with depth, from 1.3 ‰ at the surface to 2.3 ‰ at 10.8–12.0 cm (Fig. 6). At depth, the $\delta^{60}Ni$ values at the Soledad site are higher compared with the typical seawater $\delta^{60}Ni$ value (+1.3 ‰; Fig. 6, Table S3; Cameron and Vance, 2014; Takano et al., 2017; Wang et al., 2019; Archer et al., 2020; Yang et al., 2020; Lemaitre et al., 2022).

3.2. Oxic stations: Catalina Basin, San Clemente and Patton Escarpment

The oxic stations on the California continental margin (Catalina Basin, San Clemente and Patton Escarpment) have bottom water oxygen concentrations that generally increase with decreasing TOC. The Catalina Basin site has a higher TOC content (around 5 wt% TOC) compared with the other two oxic stations (around 3 and 1% TOC; Fig. 2; Table S2). In contrast to the Catalina Basin site, the San Clemente and Patton Escarpment sites show solid phase enrichments of Mn and Ni in the surface sediment (Mn/Al = 1.08 and 0.13 ppm/ppm, Ni/Al * 10^{-3} = 2.96 and 12.6 ppm/ppm; Fig. 4). The authigenic Ni fraction contributes >74% of Ni (Table S2).

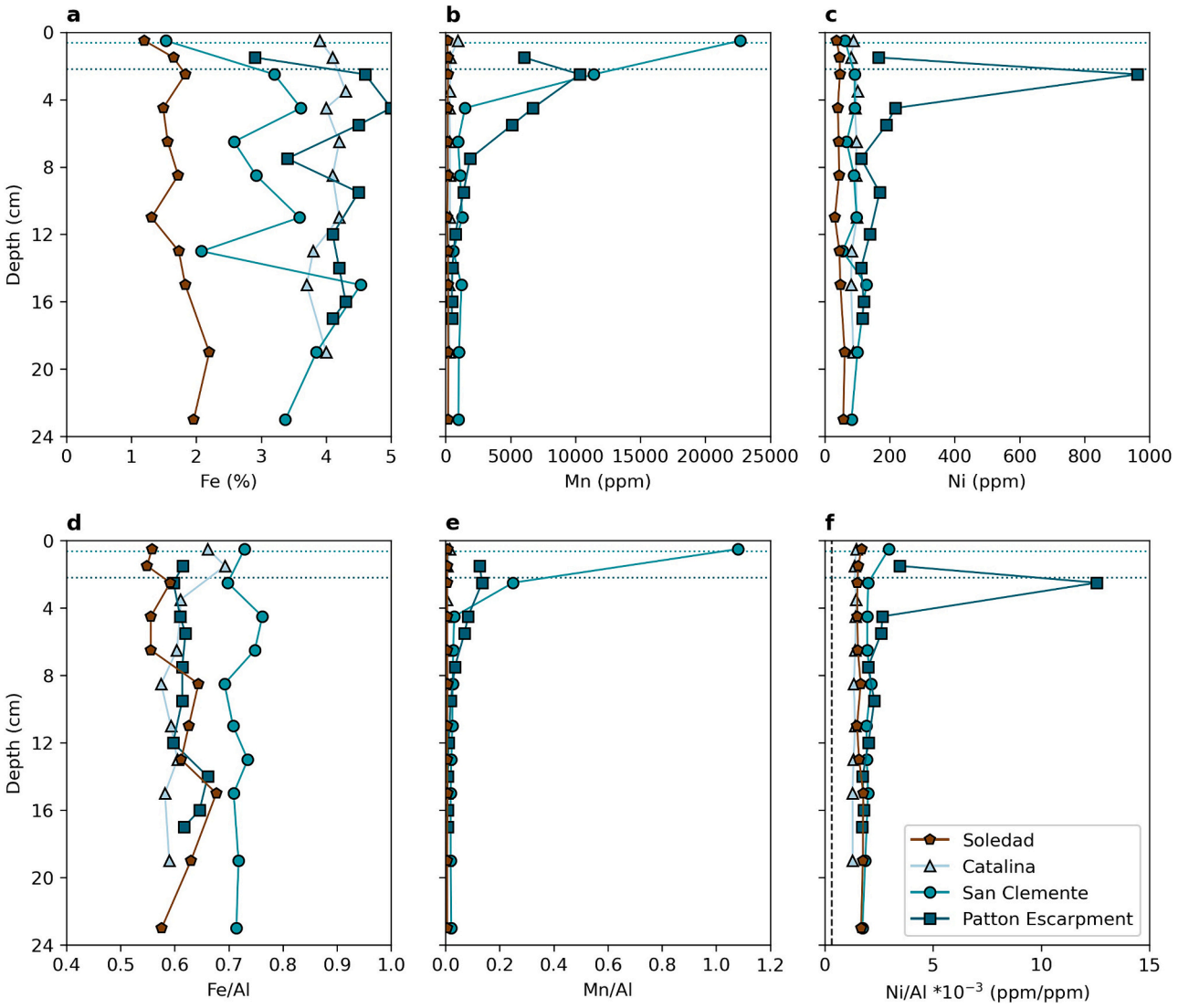

Fig. 4. Solid-phase distribution of the Fe, Mn, and Ni to Al ratio, plotted as functions of sediment depth at a) to c) the anoxic station (Soledad), and d) to f) the oxic stations (Catalina, San Clemente, Patton Escarpment). The horizontal dotted lines in d) to f) indicate the oxygen penetration depth at San Clemente (upper line) and Patton Escarpment (lower line). The vertical dashed line indicates the highest estimate of detrital Ni/Al ($3.3 * 10^{-4}$ (ppm/ppm); Böning et al., 2012). Please note that the x-axis scales of b) and c) differ from those in e) and f).

The San Clemente and Patton Escarpment stations have dissolved Mn concentrations that increase with depth to maximum values of 90 μM and 14 μM, respectively (Fig. 5; Table S3). In line with dissolved Mn, dissolved Ni concentrations at all oxic stations increase with depth, reaching a concentration maximum of nearly 500 nM at the Patton Escarpment (Fig. 6). Dissolved Fe concentrations below ~7 cm at the Catalina site (~21 μM) are higher than at the San Clemente site (~7 μM), whereas at the Patton Escarpment, dissolved Fe is consistently below 1 μM (Fig. 5; Table S3). The Ni MAR at Catalina Basin, San Clemente and Patton Escarpment are 22, 21 and 16 nmol cm^{-2} y^{-1}, respectively (Table 2). Fluxes of Ni are directed out of the sediment at San Clemente and Catalina Basin (−3.5 and − 0.8 nmol cm^{-2} y^{-1}, respectively). The Ni burial efficiency is lowest at the San Clemente site (0.86), compared to values of 0.96 or higher for the other two oxic sites (Table 2). In contrast, a small Ni flux into the sediment is suggested at Patton Escarpment (0.2 nmol cm^{-2} y^{-1}). The δ^{60}Ni values in the dissolved phase decrease with depth at all oxic stations, with the most pronounced shift in δ^{60}Ni values at Patton Escarpment (+1.88 ‰ at the surface and approximately −0.13 ‰ at depth; Fig. 6; Table S3).

4. Discussion

Our data highlight a striking difference in the behaviour of Ni under intermediate geochemical conditions when the sediments are neither highly reducing nor fully oxic. This difference is illustrated in Fig. 3, where samples from Soledad are aligned with an array of data exhibiting a positive correlation between Ni and TOC. In contrast, the data from the oxic stations fall off this trend, implying that under the conditions at these sites, other processes drive Ni cycling. The plot of δ^{60}Ni values as a function of dissolved Ni concentrations in pore fluids (Ln(Ni)) further highlights the fact that Ni isotope fractionation at these sites is influenced by other processes than those dominant at the Soledad site (Supplementary Material Fig. S1).

4.1. Soledad: the behaviour of Ni under C_{org}-rich reducing conditions

The thesis that Ni is associated with organic matter is consistent with the importance of Ni for biological processes, and is borne out through observations demonstrating a strong co-variance between these two constituents in marine sediments beneath productive upwelling settings (e.g., Böning et al., 2015; Ciscato et al., 2018; Plass et al., 2021; He et al.,

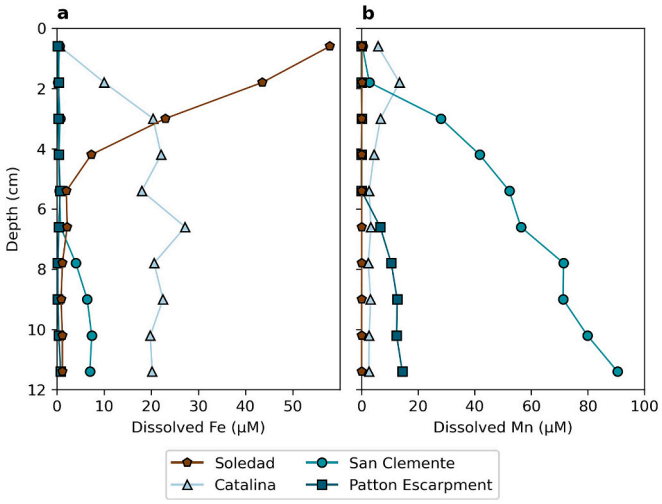

Fig. 5. Depth plots (below sediment-water interface) showing the distributions of a) Fe and b) Mn in the dissolved phase.

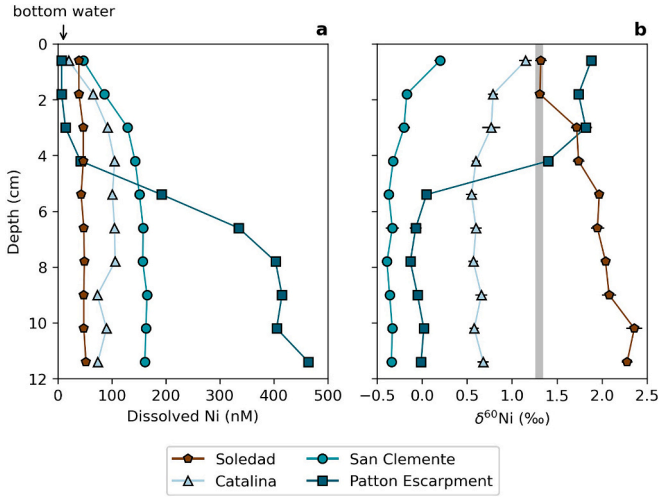

Fig. 6. a) Nickel concentrations and b) isotope compositions in the dissolved phase, plotted as a function of sediment depth. The error bars in b) are ±2σ. The typical Ni concentration of bottom water is indicated with the arrow in a), the δ^{60}Ni value typical for seawater in b) is illustrated as vertical grey bar (+1.3 ‰; Cameron and Vance, 2014; Takano et al., 2017; Wang et al., 2019; Archer et al., 2020).

2023). Indeed, Ni to TOC ratios for Soledad sediments, ranging between ~100 and 200 μmol/mol, are similar to previously published data that range between 120 and 200 μmol/mol (Table S2; Fig. 3; Böning et al., 2015; Ciscato et al., 2018; He et al., 2023). These ratios are significantly higher than the Ni:C ratio in phytoplankton from the Equatorial Pacific (6 and 12 μmol/mol; Twining et al., 2011), which is most likely caused by loss of C during respiration, both in the water column and the sediment (Böning et al., 2015; Ciscato et al., 2018; Plass et al., 2021). Soledad sediment Ni/TOC ratios show an increase with depth (Fig. 7a), a pattern that is similar to that observed along the Peruvian Margin by Böning et al. (2015). These authors conclude that the increase in Ni/TOC with sediment depth results from the preferential accumulation and preservation of Ni over TOC during the degradation of C_{org} during early diagenesis (Böning et al., 2015; Ciscato et al., 2018; Plass et al., 2021). Preferential retention of Ni in the sediment compared with TOC is consistent with the observation reported here that the burial efficiency of Ni is >90% at the Soledad station whereas C_{org} burial efficiencies are typically much lower than this value along continental margins (e.g., Berelson et al., 1996; Table 2). This hypothesis is also consistent with the fact that Ni/Al ratios barely change down core at the Soledad site (Fig. 4). We note that the detrital sediment fraction contributes a maximum of around 20% to the total Ni (Table S2). Compared to the Ni/Al ratios, the Ni concentrations show an increase downcore (from 36.6 to a maximum of 61.4 ppm at 18 to 20 cm sediment depth; Table S2).

Even though the change in solid phase Ni concentrations with

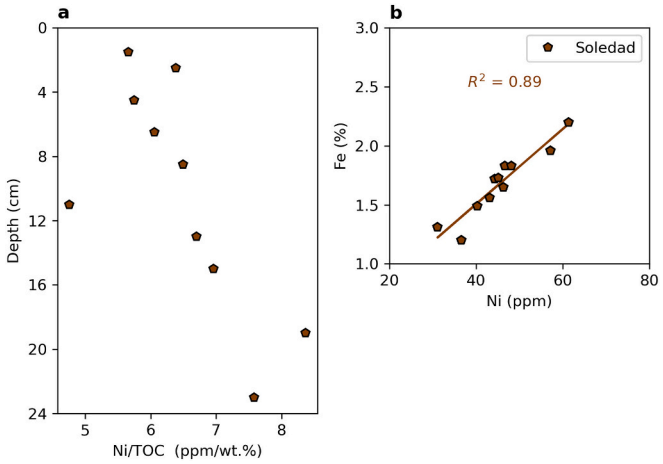

Fig. 7. Depth plot of a) Ni/TOC (ppm/wt%), showing that Ni/TOC increases with depth, and suggesting that Ni is more prone to accumulate in the sediment compared to TOC. The crossplot b) shows that Ni is positively correlated with Fe in sediments.

Table 2
Benthic fluxes, MAR and burial rates of Ni.

Station	C_0[a]	M1	M2	Φ[b]	T	$D_{sediment}$[c]	Flux	MAR[d]	Ni[e]	Ni MAR	Ni burial efficiency[f]	Flux out relative to input
	nmol m^{-3}	nmol m^{-3}	cm		°C	10^{-6} cm^{-2} s^{-1}	nmol cm^{-2} y^{-1}	mg cm^{-2} y^{-1}	μg/g	nmol cm^{-2} y^{-1}		%
Soledad	10	38.94	1	0.94	4	3.28	−2.82	50	42.9	36.5	0.93	7.7
Catalina Basin	10	19.72	1	0.89	4	2.99	−0.82	14	93.2	22.2	0.96	3.7
San Clemente	10	46.59	1	0.93	4	3.22	−3.46	15	81.0	20.7	0.86	16.7
Patton Escarpment	10	7.35	1	0.93	1.5	2.90	0.23	3	303	15.5	1.01	−1.5

[a] approximation; Bruland, 1980 in Archer et al., 2020.
[b] McManus et al., 2005, Soledad estimated based on McManus et al., 2005.
[c] $D_{seawater}$ at 25 °C = 6.79 10^{-6} cm^{-2} s^{-1} (Li and Gregory, 1974).
[d] MAR = sediment mass accumulation rate; McManus et al., 2006; Poulson et al., 2006.
[e] average of upper 10 cm.
[f] calculated as the Cr MAR divided by the MAR minus the benthic flux.

sediment depth is small, the elevated porewater concentrations relative to bottom water (39–52 nM versus 10 nM, respectively; Fig. 6) at Soledad imply that Ni is undergoing diagenetic remobilisation within the sediment. Given the strong association of solid phase Ni with TOC, it is likely organically-bound Ni, released into the pore fluid dissolved phase during organic carbon remineralisation, that is the source of this additional porewater Ni (He et al., 2023). However, this source of Ni is unlikely to control porewater isotope compositions. The surface pore fluid shows a δ^{60}Ni value of approximately 1.3 ‰ (Fig. 6), which is comparable with typical seawater (1.3 ‰; Cameron and Vance, 2014; Takano et al., 2017; Wang et al., 2019; Archer et al., 2020; Yang et al., 2020; Lemaitre et al., 2022). Deeper samples are enriched in the heavier isotope (up to 2.36 ‰; Fig. 6). Given that seawater Ni taken up into cells in the photic zone is delivered to the sediment with a negligible isotope fractionation (Ciscato et al., 2018; He et al., 2023), the heavy isotope compositions of Soledad porewaters cannot be explained by an organic matter source and are likely due to isotope fractionation during a superimposed removal process.

Dissolved Ni, from organic or inorganic sources, can be fixed in solid sulfide phases (e.g., Landing and Lewis, 1991; Vance et al., 2016). Thus, Ni that is delivered to the sediment with organic matter can be redistributed to pore fluids, from which a proportion is retained in the sediment in an alternative phase as suggested by Ciscato et al. (2018) and recently confirmed by He et al. (2023). The positive correlation between solid-phase Fe and Ni at the Soledad site (Fig. 7b) supports the thesis that Ni can be incorporated into a solid sulfide phase. At the Soledad site the dissolved Fe decrease with depth and increase in H_2S produces a solid phase Fe-sulfide diagenetic sink (up to 42 μM at 9.5 cm; Chong et al., 2012). The fact that the distribution of Ni does not appear to follow that of Fe-sulfide is likely simply due to the presence of two different processes competing to control porewater Ni concentrations: the organic matter source and the sulfide sink. Finally, the heavy Ni isotope compositions of deep porewaters is also consistent with the notion that a proportion of dissolved pore fluid Ni is incorporated into a solid sulfide phase, as this process preferentially removes isotopically light Ni, leaving the dissolved phase enriched in heavy Ni isotopes (Vance et al., 2016; He et al., 2023).

The fact that there is significant Ni in porewaters that is diagenetically mobilised from sediment is not inconsistent with relatively constant Ni abundances in sediment: this feature simply reflects the overwhelming importance in the overall mass balance of the solid pool relative to porewater. For example, given minimum observed Ni concentrations in sediment, maxima in porewaters and maximum observed porosity, the solid phase holds >99.9% of the total sediment-porewater Ni. Furthermore, while the porewaters exhibit significant variability in Ni isotope compositions, this mass balance implies that the differential isotope partitioning between the solid and dissolved pool cannot be important for the Ni isotope composition of the sediment. Diffusion of heavy porewater Ni across the sediment-water interface may, however, be important for the overlying water column. On the other hand, only approximately 8% of the input flux of Ni is released back to the bottom water (Table 2). This small benthic efflux, coupled with the fact that the near-surface dissolved Ni isotope values are identical to seawater, suggests that this process may be too insignificant to impact the marine Ni isotope balance.

4.2. The behaviour of Ni under Mn-rich oxidising conditions

Sediments deposited under conditions where Mn oxides deliver a significant amount of Ni to the sediment, and where they play a significant role in C_{org} oxidation, show marked differences to those at the Soledad site. The most obvious distinction is that the sediment Ni and TOC data for these stations are shifted off the trendline found for other sites, towards higher Ni and/or lower TOC concentrations (Fig. 3). We note that these stations have oxygenated bottom waters, but at none of the sites is oxygen present below ~3 cm in the sediment column. At San Clemente and Patton Escarpment, there are distinct near-surface enrichments in solid-phase Ni, occurring along with peaks in solid-phase Mn (Figs. 4 and 8). While the solid-phase Mn/Al and Ni/Al concentrations are correlated at the Patton Escarpment and San Clemente sites (R^2 = 0.51 and 0.90), they do not correlate as a whole (Fig. 8a). Enrichments of Ni along with Mn in the oxygenated surface sediment have previously been observed at San Clemente and Patton Escarpment, respectively; Berelson et al., 1996; Fleischmann et al., 2023). Due to the availability of oxygen in the overlying water column and the shallow oxygen penetration depth, Mn oxides precipitate in the surface sediment of these sites. Consequently, Ni has been proposed to be fixed in the solid phase by sorption onto Mn oxides (e.g., Shaw et al., 1990). In contrast to the San Clemente and Patton Escarpment sites, there are no enrichments in solid phase Ni and Mn at the Catalina site. Here, Mn oxides are restricted to the uppermost 0.3 cm of the sediment column, as evidenced by slightly elevated Mn and Ni concentrations at a sediment depth of 0–1.2 cm. Below that depth, Mn oxides are reductively dissolved and thus, not preserved in the deeper sediment record. Comparing with published data, our data from the Patton Escarpment typically fall close to data from abyssal sediments (Fig. 8b; Fleischmann et al., 2023). Furthermore, the San Clemente station falls in the group of sediments from the California margin with high C_{org} contents and reductive mobilisation of Mn as identified by Fleischmann et al. (2023; Fig. 8b). These authors note that Mn oxides and associated Ni are differentially re-processed during diagenesis. Following the mobilisation of Mn and Ni under reducing conditions at depth and upward Ni and Mn diffusion, Mn is enriched in the solid phase in the oxygenated surface sediment, whereas Ni can be lost to the water column

In the surface sediments of the San Clemente and Patton Escarpment sites, dissolved Ni concentrations are lower compared with deeper samples. This pattern reflects deeper remobilisation of Ni from Mn oxides. In short, where the conditions in the sediment become anoxic, Mn oxides dissolve, releasing Ni along with Mn from the solid to the dissolved phase (as suggested by Shaw et al., 1990). This upward diffusion transports dissolved Ni into the oxygenated surface sediment, where Ni can be released to the bottom water or removed from solution by (re-) adsorption onto precipitating Mn oxides (Koschinsky and Hein, 2003; Peacock and Sherman, 2007; Peacock, 2009; Gall et al., 2013). Thus, the maxima of solid-phase Ni/Al in the surface sediments of the San Clemente and Patton Escarpment sites are caused by a combination of Ni input from the water column and recycled Ni from deeper in the sediment, likely from both Mn oxide dissolution and organic matter remineralisation at depth followed by upward diffusion. The absence of a relationship between either dissolved or solid Ni and Mn at the Catalina Basin site is likely because most of the solid-phase reactive Mn, which is a primary carrier of Ni, is dissolved and lost to the overlying water column. This Mn dissolution is because dissolved oxygen is less than half the concentration at the Catalina Basin (20 μM) as compared to San Clemente (50 μM), thus initiating Mn reduction much shallower within the sediment column or even within the water column at Catalina Basin.

Like the solid phase relationships between Mn and Ni, their dissolved concentrations also correlate at each site (R^2 = 0.82 or higher; Fig. 8c). Dissolved Ni concentrations stabilise at 3.6–4.8 cm sediment depth at around 157 ± 8 nM (SD, n = 7) at the San Clemente site, and at 7.2–8.4 cm depth at the Patton Escarpment site (422 ± 57 nM (SD, n = 4), while dissolved Mn concentrations increase steadily with depth. Despite the near-surface solid Mn peak, a proportion of dissolved Mn diffuses from sediment into the bottom water (McManus et al., 2012). In addition, efflux of Mn is influenced by the oxidation of C_{org}, since Mn can be scavenged by organic matter (Johnson et al., 1996; McManus et al., 2012). Consequently, Mn can be partially lost to the bottom water, instead of being quantitatively trapped within the sediment column by repetitive cycles of precipitation and dissolution below the water-sediment interface (recycling). The Ni benthic flux out of the sediment at the San Clemente site (−3.5 nmol cm^{-2} y^{-1}) is higher compared with the other sites studied here (Table 2). Based on this benthic Ni flux, we

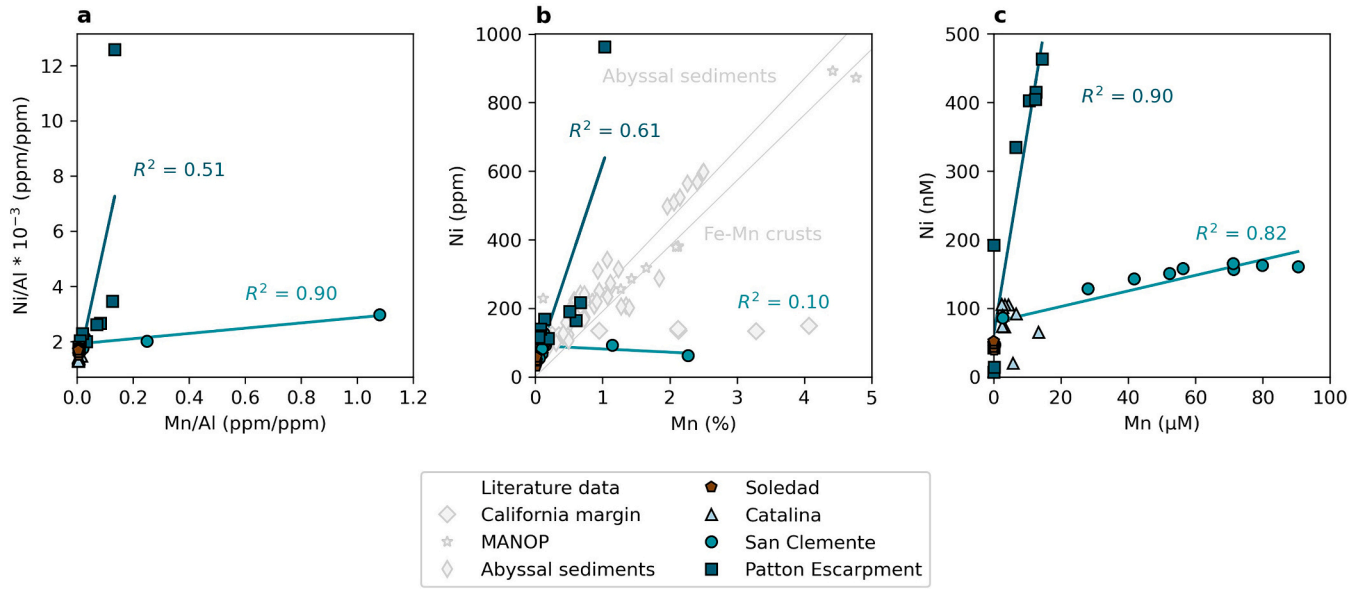

Fig. 8. Ratios of solid Mn and Ni and b) concentrations of dissolved Mn and Ni, showing the positive correlations of Ni and Mn at the San Clemente and Patton Escarpment sites. The literature data in a) are from Fleischmann et al. (2023) for California Margin and abyssal sediments, and from Little et al. (2020) for MANOP sediments (Fe—Mn crusts). The slopes of abyssal sediments and Fe—Mn crusts as described in Fleischmann et al. (2023) are indicated by thin grey line.

suggest that Ni is partially released to the bottom water resulting in a lower burial efficiency (0.86) than at all our other stations (Table 2). This contribution of Ni may impact the dissolved seawater Ni pool as well as its isotope composition.

While we find evidence for the accumulation of Ni in the solid phase along with Mn oxides at both the San Clemente and Patton Escarpment sites, Ni and Mn show distinct behaviours as described by Fleischmann et al. (2023). While the solid-Ni peak is most pronounced in the sediments of the Patton Escarpment, the peak in solid-phase Mn at this site is smaller than the one at the San Clemente Basin site (Fig. 4). The differing behaviours of sediment Ni and Mn can result from preferential loss of Mn compared with Ni from the solid to the dissolved phase at the Patton Escarpment. The overall down-core trend of higher solid-phase Ni/Mn ratios is more pronounced at Patton Escarpment than in San Clemente (Fig. S2, Supplementary Information). Similar to the observations here, Little et al. (2020) found that due to Mn reduction, Mn may be more prone to loss from the sediment package compared to Ni during cycles of dissolution and reprecipitation of Mn oxides and this effect of Mn diagenesis is apparent to varying degrees along the continental margins studied here. In addition, non-quantitative trapping of Ni from pore fluids to reprecipitating Mn oxides in the oxygenated surface sediment can result in lower sediment Ni/Mn ratios compared with deeper samples (Fleischmann et al., 2023). Hence, at the San Clemente site, where the oxygen penetration depth is shallower than at the Patton Escarpment site, the proportion of Ni that escapes trapping by Mn oxides is larger. Consequently, Ni is diffusing out of the sediment package, whereas at the Patton Escarpment site, the burial of Ni in the sediment is more efficient and leads to the high Ni/Al * 10^{-3} ratios (Fig. 4). It is likely that the relatively deep oxygen penetration depth at the Patton Escarpment allows the preservation of Mn oxides in the surface sediment, forming a "lid" that prevents dissolved fluxes from escaping to the bottom water.

An additional influence on the behaviour of Ni and Mn at the San Clemente and Patton Escarpment sites, could relate to the behaviour of Mn linked to its mineralogy (Little et al., 2020; Fleischmann et al., 2023). Though the effect may be subtle, and difficult to deconvolve from other controls, the formation of todorokite from birnessite leads to the preferential loss of Ni compared to Mn from the sediment (Atkins et al., 2016; Little et al., 2020). During todorokite transformation, Ni is not significantly incorporated in the crystal structure, and can thus be transferred to the pore fluid (Atkins et al., 2016). At the Patton Escarpment site, the conditions are more oxidising compared to the San Clemente site. Environments with lower oxidation potential favour todorokite formation (McMurtry, 2009; Wegorzewski et al., 2020). Therefore, it is possible that more todorokite is present at the San Clemente compared with the Patton Escarpment site, since the former has a lower bottom water oxygen concentration and shallower oxygen penetration depth (Table 1). Thus, the mineralogy may explain the preferential retention of Mn at the San Clemente site. We recognise that this mineralogical explanation is speculative as we do not have information on the abundance of todorokite in our samples.

The oxygenated surface pore fluids are enriched in heavier Ni compared with the Ni isotope composition in the pore fluids deeper in the sediment at the San Clemente and Patton Escarpment sites (Fig. 6), whereby surface pore fluids show the highest δ^{60}Ni values at the Patton Escarpment site (up to 1.88 ‰; Fig. 6; Table S3). The net Ni isotope shift from the interface (0–1.2 cm) to 10.8–12.0 cm sediment depth is −0.55 ‰ for San Clemente, and − 1.88 ‰ for Patton Escarpment. These shifts likely result from the repetitive cycling of Ni associated with Mn oxides or the mineralogy of the Mn as described above, or a combination thereof. Both of these processes eventually shift the δ^{60}Ni of the pore fluid towards higher values (Little et al., 2020; Sorensen et al., 2020; Chen et al., 2022; Fleischmann et al., 2023). Isotopically light Ni preferentially sorbs onto (re-) precipitating Mn oxide, leaving the remaining pore fluids in the oxygenated upper few cm of the sediment column enriched in heavy Ni isotopes (Little et al., 2020; Sorensen et al., 2020). In addition, Ni desorbing from Mn oxides during early diagenesis is isotopically heavier compared with the remaining solids, as previously suggested by Little et al. (2020). During the transformation of birnessite to todorokite, the latter mineral retains isotopically light Ni, whereas isotopically heavy Ni is released into the pore fluid (Chen et al., 2022).

To distinguish between the influence of Mn cycling on Ni and the degree of structural incorporation of Ni into birnessite and isotopic re-equilibration, Fleischmann et al. (2023) utilise Co/Mn ratios. While the flux of Co to the sediment is nearly constant (Halbach et al., 1983), Co can diffuse from the sediment under reducing conditions (e.g., Shaw et al., 1990; Tagliabue et al., 2018; Plass et al., 2021). During the transformation of birnessite to todorokite, Co is retained in the solid phase (Wu et al., 2019). Due to this behaviour of Co, samples that underwent diagenetic redox processing fall off a trendline of positively correlated sediment δ^{60}Ni values and Co/Mn ratios towards lower or

higher Co/Mn (Fleischmann et al., 2023). Along with the data presented by Fleischmann et al. (2023) for the California margin, the sediment samples from the San Clemente Basin fall along a trend line between Co/Mn and Ni/Mn (Fig. S3), reflecting that Ni cycling is strongly linked to Mn redox processes in these sediments.

The δ^{60}Ni values in Catalina Basin are shifted towards higher δ^{60}Ni values throughout the core compared with San Clemente, with surface δ^{60}Ni values similar to the ones at the Soledad, but lower than the Patton Escarpment site (Fig. 6). In addition, the C_{org} burial rate at the Catalina site is slightly higher (1.2 mmol m^{-2} d^{-1}; Table 1) compared with the one at the San Clemente site (0.9 mmol m^{-2} d^{-1}), but still much lower than at Soledad (8.4 mmol m^{-2} d^{-1}). The δ^{60}Ni values of Catalina Basin pore fluids are thus likely influenced by a combination of weak redox cycling of Mn oxides due to the shallow oxygen penetration depth (0.33 cm; Berelson et al., 1996), and, to a lesser extent, delivery of Ni to the sediment with organic matter and subsequent release of isotopically heavy Ni to the pore fluid.

The benthic Ni flux out of the sediment at the San Clemente site is larger compared to all other stations (−3.46 nmol cm^{-2} y^{-1}; Table 2). The Ni isotope composition of this flux is thought to be similar to the δ^{60}Ni values of the surface pore fluids, 0.2 ‰, and thus isotopically lighter than typical seawater (+1.3 ‰; Cameron and Vance, 2014; Takano et al., 2017; Wang et al., 2019; Archer et al., 2020). Similarly, at the Catalina site, the benthic flux likely has a δ^{60}Ni value similar to the surface pore fluid sample and thus lower than seawater (1.15 ‰). However, the benthic flux at the Catalina Basin site is high (−0.8 nmol cm^{-2} y^{-1}), and also the burial efficiency is high (0.96). For the Patton Escarpment site, our benthic flux calculations (0.23 nmol cm^{-2} y^{-1}; Table 2) as well as the calculated burial efficiency (1.01), predict that this isotopically heavy Ni is not released to the bottom water, but preserved within the sediment record. As a consequence of the high burial efficiency, repeated cycles of Mn oxide formation and dissolution lead to the progressive enrichment of isotopically heavy Ni in the Patton Escarpment surface pore fluid (up to 1.88 ‰). In contrast, at the San Clemente site, some of the dissolved Ni escapes to the bottom water, resulting in a weaker enrichment of isotopically heavy Ni (only up to 0.2 ‰) than observed at the Patton Escarpment site. Even though the burial efficiencies at the oxic sites studied here vary, all of them are >0.85, and the range overlaps with the burial efficiency at the sulfidic site (Soledad). Thus, Ni is well-preserved in the sediment column of all stations studied here.

5. Conclusions

In this study, we provide new insights on Ni cycling across the sediment-water boundary and during early diagenesis under intermediate redox conditions. Under C_{org}-rich conditions at the Soledad site, Ni is effectively retained in the sediment, having a burial efficiency of >90%. Based on pore fluid results, Ni is partially removed to the sediment in an authigenic sulfide phase, whereby isotopically light Ni is likely preferentially bound to sulfides. The δ^{60}Ni values of the remaining pore fluid show an increase from seawater-like values at the surface to 2.28 ‰ at depth, the most enriched in heavy Ni of all the sites studied here. Given the fact that the solid phase overwhelmingly dominates the mass balance of the sediment-porewater system, these isotope fractionations that control porewater will have no significant impact on the Ni finally buried at highly reducing sites like Soledad, as previously concluded for the Namibia margin (He et al., 2023). Further, the recycling efficiency of Ni at this site is low and the pore fluid δ^{60}Ni value is close to seawater near the sediment-water boundary. Under these types of conditions, diagenesis probably does not significantly impact the global Ni recycling inventory or its isotope composition.

Under conditions where the near-surface sediment is Mn-rich, Ni's distribution and its isotope fractionation appear linked to Mn dissolution and reprecipitation. Under these conditions, Ni accumulates in the solid phase by sorption onto Mn oxides, and is released by reductive dissolution of Mn oxides deeper in the sediment column. Our data indicate that isotopically light Ni is preferentially retained in the sediment along with Mn oxides, whereas isotopically heavy Ni is preferentially released to the pore fluids, confirming previous findings (e.g., Little et al., 2020; Fleischmann et al., 2023). A shallow oxygen penetration depth at San Clemente leads to a Ni benthic flux out of the sediment of −3.46 nmol cm^{-2} y^{-1}, and this Ni isotope composition is lower than typical seawater. In contrast, a deep oxygen penetration depth (Patton Escarpment) facilitates the formation of a Mn oxide layer in the surface sediment, preventing the significant release of isotopically heavy Ni from pore fluids to bottom water. Under these conditions, Ni burial in the sediment is highly efficient with all (or nearly all) Ni being retained within the sediment.

It is noteworthy that the Ni burial efficiencies are similar to each other at all stations investigated here, even though the processes driving Ni cycling differ between the sulfidic Soledad (linked to the C cycle) site and the manganous sites (Table 2). The utility of this observation is that for Ni concentrations or isotope compositions to serve as tracers for biogeochemical conditions of the past oceans, it is important that Ni is well preserved following deposition.

CRediT authorship contribution statement

Sylvie Bruggmann: Writing – review & editing, Writing – original draft, Visualization, Validation, Methodology, Investigation, Formal analysis, Data curation, Conceptualization. **James McManus:** Writing – review & editing, Supervision, Resources, Project administration, Methodology, Funding acquisition, Conceptualization. **Corey Archer:** Writing – review & editing, Validation, Supervision, Methodology, Formal analysis, Data curation. **Derek Vance:** Writing – review & editing, Validation, Supervision, Resources, Project administration, Funding acquisition, Data curation. **Silke Severmann:** Writing – review & editing, Validation, Supervision, Resources, Project administration, Methodology, Funding acquisition, Formal analysis, Conceptualization.

Declaration of competing interest

The authors declare that they have no known competing financial interests or personal relationships that could have appeared to influence the work reported in this paper.

Data availability

All data are available in the supplementary material.

Acknowledgements

We are thankful to the members of the crew and the researchers for their support during sample collection at sea. Further, we would like to thank Sara Rauschenberg, Miguel Angel Huerta-Diaz, Dominique Iaccarino and William Biggs for their assistance in sample collection, preparation and analysis. This work was supported by the NSF [grant numbers OC-1657832 to JM and OC-1657690 to SS], and the SNF [grant number 200021_184873 to DV]. JM was supported during his employment while at the National Science Foundation. The findings and opinions represented here do not reflect those of the National Science Foundation.

Appendix A. Supplementary data

Supplementary data to this article can be found online at https://doi.org/10.1016/j.chemgeo.2024.122234.

References

Archer, C., Vance, D., Milne, A., Lohan, M.C., 2020. The oceanic biogeochemistry of nickel and its isotopes: new data from the South Atlantic and the Southern Ocean biogeochemical divide. Earth Planet. Sci. Lett. 535, 116118.

Atkins, A.L., Shaw, S., Peacock, C.L., 2016. Release of Ni from birnessite during transformation of birnessite to todorokite: implications for Ni cycling in marine sediments. Geochim. Cosmochim. Acta 189, 158–183.

Barnett, P.R.O., Watson, J., Connelly, D., 1984. A multiple corer for taking virtually undisturbed samples from shelf, bathyal, and abyssal sediments. Oceanol. Acta 7, 399–408.

Berelson, W.M., Hammond, D.E., Johnson, K.S., 1987. Benthic fluxes and the cycling of biogenic silica and carbon in two southern California borderland basins, United States. Geochim. Cosmochim. Acta 51, 1345–1363.

Berelson, W.M., McManus, J., Coale, K.H., Johnson, K.S., Kilgore, T., Pilskaln, C., 1996. Biogenic matter diagenesis on the sea floor: a comparison between two continental margin transects. OEAS Fac. Publ. 138, 731–762.

Böning, P., Fröllje, H., Beck, M., Schnetger, B., Brumsack, H.-J., 2012. Underestimation of the authigenic fraction of Cu and Ni in organic-rich sediments. Mar. Geol. 323-325, 24–28.

Böning, P., Shaw, T., Pahnke, K., Brumsack, H.J., 2015. Nickel as indicator of fresh organic matter in upwelling sediments. Geochim. Cosmochim. Acta 162, 99–108.

Boudreau, B.P., 1996. Diagenetic Models and their Implementation. Springer, Heidelberg.

Boyle, E.A., Huested, S.S., Jones, S.P., 1981. On the distribution of copper, nickel, and cadmium in the surface waters of the North Atlantic and North Pacific Ocean. J. Geophys. Res. Oceans 86, 8048–8066.

Bruggmann, S., Severmann, S., McManus, J., 2023. Geochemical conditions regulating chromium preservation in marine sediments. Geochim. Cosmochim. Acta 348, 239–257.

Bruland, K.W., 1980. Oceanographic distributions of cadmium, zinc, nickel, and copper in the North Pacific. Earth Planet. Sci. Lett. 47, 176–198.

Cameron, V., Vance, D., 2014. Heavy nickel isotope compositions in rivers and the oceans. Geochim. Cosmochim. Acta 128, 195–211.

Chen, L., Archer, C., Little, S.H., Peacock, C.L., 2022. An Isotopically Heavy Source of Nickel: Release of Nickel During Birnessite Transformation into Todorokite (Goldschmidt Conference).

Chong, L.S., Prokopenko, M.G., Berelson, W.M., Townsend-Small, A., McManus, J., 2012. Nitrogen cycling within suboxic and anoxic sediments from the continental margin of Western North America. Mar. Chem. 128–129, 13–25.

Ciscato, E.R., Bontognali, T.R.R., Vance, D., 2018. Nickel and its isotopes in organic-rich sediments: implications for oceanic budgets and a potential record of ancient seawater. Earth Planet. Sci. Lett. 494, 239–250.

Fleischmann, S., Du, J., Chatterjee, A., McManus, J., Iyer, S.D., Amonkar, A., Vance, D., 2023. The nickel output to abyssal pelagic manganese oxides: a balanced elemental and isotope budget for the oceans. Earth Planet. Sci. Lett. 619, 118301.

Gall, L., Williams, H.M., Siebert, C., Halliday, A.N., Herrington, R.J., Hein, J.R., 2013. Nickel isotopic compositions of ferromanganese crusts and the constancy of deep ocean inputs and continental weathering effects over the Cenozoic. Earth Planet. Sci. Lett. 375, 148–155.

Gueguen, B., Rouxel, O., 2021. The nickel isotope composition of the authigenic sink and the diagenetic flux in modern oceans. Chem. Geol. 563, 120050.

Gueguen, B., Rouxel, O., Fouquet, Y., Ponzevera, E., Bekker, A., 2013. Nickel isotope variations in terrestrial silicate rocks and geological reference materials measured by MC-ICP-MS. Geostand. Geoanal. Res. 37, 297–317.

Gueguen, B., Rouxel, O., Rouget, M., Bollinger, C., Ponzevera, E., Germain, Y., Fouquet, Y., 2016. Comparative geochemistry of four ferromanganese crusts from the Pacific Ocean and significance for the use of Ni isotopes as paleoceanographic tracers. Geochim. Cosmochim. Acta 189, 214–235.

Gueguen, B., Sorensen, J.V., Lalonde, S.V., Peña, J., Toner, B.M., Rouxel, O., 2018. Variable Ni isotope fractionation between Fe-oxyhydroxides and implications for the use of Ni isotopes as geochemical tracers. Chem. Geol. 481, 38–52.

Halbach, P., Segl, M., Puteanus, D., Mangini, A., 1983. Co-fluxes and growth rates in ferromanganese deposits from Central Pacific seamount areas. Nature 304 (5928), 716–719.

He, Z., Archer, C., Yang, S., Vance, D., 2023. Sedimentary cycling of zinc and nickel and their isotopes on an upwelling margin: Implications for oceanic budgets and paleoenvironment proxies. Geochim. Cosmochim. Acta 343, 84–97.

Hein, J.R., Yeh, H.W., Alexander, E., 1979. Origin of iron-rich montmorillonite from the manganese nodule belt of the North Equatorial Pacific. Clay Clay Miner. 27, 185–194.

John, S.G., Kelly, R.L., Bian, X., Fu, F., Smith, M.I., Lanning, N.T., Liang, H., Pasquier, B., Seelen, E.A., Holzer, M., Wasylenki, L., Conway, T.M., Fitzsimmons, J.N., Hutchins, D.A., Yang, S.C., 2022. The biogeochemical balance of oceanic nickel cycling. Nat. Geosci. 15 (11), 906–912.

Johnson, K.S., Coale, K.H., Berelson, W.M., Gordon, R.M., 1996. On the formation of the manganese maximum in the oxygen minimum. Geochim. Cosmochim. Acta 60, 1291–1299.

Koschinsky, A., Hein, J.R., 2003. Uptake of elements from seawater by ferromanganese crusts: solid-phase associations and seawater speciation. Mar. Geol. 198, 331–351.

Landing, W.M., Lewis, B.L., 1991. Thermodynamic modeling of trace metal speciation in the Black Sea. In: NATO ASI Series. Springer, Dordrecht, pp. 125–260.

Lemaitre, N., Du, J., De Souza, G.F., Archer, C., Vance, D., 2022. The essential bioactive role of nickel in the oceans: evidence from nickel isotopes. Earth Planet. Sci. Lett. 584, 117513.

Li, Y.-H., Gregory, S., 1974. Diffusion of ions in seawater and deep sea sediments. Geochim. Cosmochim. Acta 3 (38), 703–714.

Little, S.H., Vance, D., Walker-Brown, C., Landing, W.M., 2014. The oceanic mass balance of copper and zinc isotopes, investigated by analysis of their inputs, and outputs to ferromanganese oxide sediments. Geochim. Cosmochim. Acta 125, 673–693.

Little, S.H., Archer, C., McManus, J., Najorka, J., Wegorzewski, A.V., Vance, D., 2020. Towards balancing the Oceanic Ni budget. Earth Planet. Sci. Lett. 547.

Mackey, D.J., O'Sullivan, J.E., Watson, R.J., Dal Pont, G., 2002. Trace metals in the Western Pacific: temporal and spatial variability in the concentrations of Cd, Cu, Mn and Ni. Deep-Sea Res. I Oceanogr. Res. Pap. 49 (12), 224–2259.

McManus, J., Berelson, W.M., Coale, K.H., Johnson, K.S., Kilgore, T.E., 1997. Phosphorus regeneration in continental margin sediments. Geochim. Cosmochim. Acta 61, 2891–2907.

McManus, J., Berelson, W.M., Klinkhammer, G.P., Hammond, D.E., Holm, C., 2005. Authigenic uranium: relationship to oxygen penetration depth and organic carbon rain. Geochim. Cosmochim. Acta 69, 95–108.

McManus, J., Berelson, W.M., Severmann, S., Poulson, R.L., Hammond, D.E., Klinkhammer, G.P., Holm, C., 2006. Molybdenum and uranium geochemistry in continental margin sediments: paleoproxy potential, 70, 4643–4662.

McManus, J., Berelson, W.M., Severmann, S., Johnson, K.S., Hammond, D.E., Roy, M., Coale, K.H., 2012. Benthic manganese fluxes along the Oregon-California continental shelf and slope. Cont. Shelf Res. 43, 71–85.

McMurtry, G.M., 2009. Authigenic deposits. In: Steele, J.H., Thorpe, S.A., Turekian, K.K. (Eds.), Marine Chemistry & Geochemistry: A Derivative of the Encyclopedia of Ocean Sciences, Second ed. Elsevier, Oxford, pp. 325–335.

Muratli, J.M., McManus, J., Mix, A., Chase, Z., 2012. Dissolution of fluoride complexes following microwave-assisted hydrofluoric acid digestion of marine sediments. Talanta 89, 195–200.

Peacock, C.L., 2009. Physiochemical controls on the crystal-chemistry of Ni in birnessite: genetic implications for ferromanganese precipitates. Geochim. Cosmochim. Acta 73, 3568–3578.

Peacock, C.L., Sherman, D.M., 2007. Sorption of Ni by birnessite: equilibrium controls on Ni in seawater. Chem. Geol. 238, 94–106.

Plass, A., Dale, A.W., Scholz, F., 2021. Sedimentary cycling and benthic fluxes of manganese, cobalt, nickel, copper, zinc and cadmium in the Peruvian oxygen minimum zone. Mar. Chem. 233, 103982.

Poulson, R.L., Siebert, C., McManus, J., Berelson, W.M., 2006. Authigenic molybdenum isotope signatures in marine sediments. Geology 34, 617–620.

Ragsdale, S.W., 2009. Nickel-based enzyme systems. J. Biol. Chem. 284, 18571–18575.

Sclater, F.R., Boyle, E., Edmond, J.M., 1976. On the marine geochemistry of nickel. Earth Planet. Sci. Lett. 31, 119–128.

Shaw, M., Kes, J.G.I., Nke, C.J.A., 1990. Early Diagenesis in Differing Depositional Environments: The Response of Transition Metals in Pore Water, 54, pp. 1233–1246.

Sholkovitz, E.R., 1972. The Chemical and Physical Oceanography and the Interstitial Water Chemistry of the Santa Barbara Basin. University of California.

Sorensen, J.V., Gueguen, B., Stewart, B.D., Peña, J., Rouxel, O., Toner, B.M., 2020. Large nickel isotope fractionation caused by surface complexation reactions with hexagonal birnessite. Chem. Geol. 537.

Stumm, W., Morgan, J.J., 1996. Aquatic Chemistry: Chemical Equilibria and Rates in Natural Waters, Third editions. John Wiley & Sons, Inc.

Sun, M., Archer, C., Vance, D., 2021. New methods for the chemical isolation and stable isotope measurement of multiple transition metals, with application to the earth sciences. Geostand. Geoanal. Res. 45, 643–658.

Tagliabue, A., Hawco, N.J., Bundy, R.M., Landing, W.M., Milne, A., Morton, P.L., Saito, M.A., 2018. The role of external inputs and internal cycling in shaping the global ocean cobalt distribution: insights from the first cobalt biogeochemical model. Glob. Biogeochem. Cycles 32 (4), 594–616.

Takano, S., Tanimizu, M., Hirata, T., Shin, K.-C., Fukami, Y., Suzuki, K., Sohrin, Y., 2017. A simple and rapid method for isotopic analysis of nickel, copper, and zinc in seawater using chelating extraction and anion exchange. Anal. Chim. Acta 967, 1–11.

Tribovillard, N., Algeo, T.J., Lyons, T., Riboulleau, A., 2006. Trace metals as paleoredox and paleoproductivity proxies: an update. Chem. Geol. 232, 12–32.

Twining, B.S., Baines, S.B., Bozard, J.B., Vogt, S., Walker, E.A., Nelson, D.M., 2011. Metal quotas of plankton in the equatorial Pacific Ocean. Deep Res. Part II Top. Stud. Oceanogr. 58, 325–341.

Vance, D., Little, S.H., Archer, C., Cameron, V., Andersen, M.B., Rijkenberg, M.J.A., Lyons, T.W., 2016. The oceanic budgets of nickel and zinc isotopes: the importance of sulfidic environments as illustrated by the Black Sea. Philos. Trans. R. Soc. A 374, 1–26.

Wang, R.M., Archer, C., Bowie, A.R., Vance, D., 2019. Zinc and nickel isotopes in seawater from the Indian Sector of the Southern Ocean: the impact of natural iron fertilization versus Southern Ocean hydrography and biogeochemistry. Chem. Geol. 511, 452–464.

Wegorzewski, A.V., Grangeon, S., Webb, S.M., Heller, C., Kuhn, T., 2020. Mineralogical transformations in polymetallic nodules and the change of Ni, Cu and Co crystal-chemistry upon burial in sediments. Geochim. Cosmochim. Acta 282, 19–37.

Wu, Z., Peacock, C.L., Lanson, B., Yin, H., Zheng, L., Chen, Z., Tan, W., Qiu, G., Liu, F., Feng, X., 2019. Transformation of Co-containing birnessite to todorokite: effect of Co

on the transformation and implications for Co mobility. Geochim. Cosmochim. Acta 246, 21–40.
Yang, S.-C., Hawco, N.J., Pinedo-González, P., Bian, X., Huang, K.-F., Zhang, R., John, S. G., 2020. A new purification method for Ni and Cu stable isotopes in seawater provides evidence for widespread Ni isotope fractionation by phytoplankton in the North Pacific. Chem. Geol. 547, 119662.
Yang, S.-C., Kelly, R.L., Bian, X., Conway, T.M., Huang, K.-F., Ho, T.-Y., Neibauer, J.A., Keil, R.G., Moffett, J.W., John, S.G., 2021. Lack of redox cycling for nickel in the water column of the Eastern tropical north pacific oxygen deficient zone: insight from dissolved and particulate nickel isotopes. Geochim. Cosmochim. Acta 309, 235–250.